Whitmarsh, R.B., Sawyer, D.S., Klaus, A., and Masson, D.G. (Eds.), 1996
Proceedings of the Ocean Drilling Program, Scientific Results, Vol. 149

31. MARINE WEATHERING OF SERPENTINITES AND SERPENTINITE BRECCIAS, SITES 897 AND 899, IBERIA ABYSSAL PLAIN[1]

K.L. Milliken,[2] F.L. Lynch,[2] and K.E. Seifert[3]

ABSTRACT

Low-temperature aqueous alteration (weathering) of serpentinitic basement rocks at Sites 897 and 899 has produced dramatic textural and compositional modifications. Fe-oxyhydroxides, clay minerals, and calcium carbonate fill multiple generations of brittle fractures. Replacement of serpentinite minerals by smectite, carbonate, quartz, and possibly other clay minerals was accomplished through a complex sequence of repeated dissolution and precipitation. The youngest generation of brittle fractures is filled with particulate debris, including surviving fragments of serpentinite and fragments of all of the authigenic minerals. Enrichments of relatively immobile elements in altered samples (on a carbonate-free basis) suggest volume losses, relative to the initial serpentinitic material, in excess of 50% at Site 897 and 20% at Site 899. The magnitude of Mg loss (on a carbonate-free basis) roughly confirms these apparent volume changes but is difficult to assess given possible additions of oxidized iron to these samples.

INTRODUCTION

Serpentinite basement rocks at Ocean Drilling Program (ODP) Leg 149 Sites 897 and 899 display prominent evidence of fluid/rock interaction that is visible at the macroscopic scale (Shipboard Scientific Party, 1994a, 1994b). The most highly altered basement rocks at these sites are relatively unconsolidated—capable of being manually disaggregated—in strong contrast to the less altered portions of the basement cores. Prominent yellow-orange coloration, carbonate-filled brittle fractures, open fracture porosity, and secondary dissolution of silicates all attest to a high degree of localized postserpentinization alteration. Similarly obvious alteration has been reported for other deep-sea occurrences of mafic and ultramafic rocks (e.g., Alt and Honnorez, 1984; Gillis and Robinson, 1988; Agrinier et al., 1988; Evans and Baltuck, 1988).

This paper reports further investigations into the general nature of the textural, mineralogic, and compositional modifications responsible for alteration of these serpentinized peridotites. More specific and detailed treatment of brittle fracture and precipitation of carbonate minerals in these altered rocks is the subject of separate papers on kinematic history (Morgan and Milliken, this volume), carbonate geochemistry (Milliken and Morgan, this volume), and alteration related to calcite emplacement (Gibson et al., this volume). This paper emphasizes the petrography and chemistry of reactions involving the noncarbonate components of these altered ultramafic rocks.

Petrographic, X-ray diffraction (XRD), and whole-rock elemental data reveal major chemical fluxes for several elements, involving both import and export. The mineral associations observed implicate large volumes of seawater at relatively low temperatures as the primary agent of "weathering." This example of altered serpentinites has a relatively simple and well-constrained burial history and so provides a useful analogue for understanding the textural and chemical evolution of ophicarbonates in a variety of tectonic settings.

[1]Whitmarsh, R.B., Sawyer, D.S., Klaus, A., and Masson, D.G. (Eds.), 1996. *Proc. ODP, Sci. Results,* 149: College Station, TX (Ocean Drilling Program).
[2]Department of Geological Sciences, University of Texas, Austin, TX 78712, U.S.A. kitty@maestro.geo.utexas.edu
[3]Department of Geological Sciences, Iowa State University, Ames, IA 50011, U.S.A.

SAMPLING AND METHODS

Samples were selected for this study on the basis of their extreme degree of apparent alteration, as observed in the core at the time of shipboard sampling (Table 1). Three groups of samples were collected: altered serpentinites from Holes 897C and 897D; altered serpentinite breccias from the upper portion of the Upper Breccia Unit, Hole 899B; and samples from a dark reddish, clay-rich zone in Section 149-899B-15R-5, immediately overlying the Upper Breccia Unit in Hole 899B. Relatively unaltered samples from both sites were used for comparative purposes; data for these unweathered samples are described more completely elsewhere in this volume (Seifert and Brunotte, this volume; Gibson et al., this volume).

Petrography

Polished thin sections were used for standard light microscope observation and for backscattered electron imaging of the alteration fabrics. Backscattered electron images were made on carbon-coated polished sections using 15-kV accelerating voltage and either 12- or 15-nA sample currents (measured on brass with a 10-µm spot). Additional information on clay minerals was obtained from gold-coated specimens observed in a scanning electron microscope (SEM).

X-ray Mineralogy

Whole-rock XRD data were collected from randomly oriented <50-µm powders on a Siemens D500 diffractometer. Clay analyses (air-dried and glycol solvated) were performed on the <2-µm fraction (isolated by centrifugation) following the techniques of Moore and Reynolds (1989). Calcite dissolution was accomplished by mixing the whole-rock powders with 10% acetic acid.

Elemental Chemistry

Whole-rock powders were used to obtain major element and trace-element data. The major elements Si, Ti, Al, Fe, Mn, Mg, Ca, Na, K, and P were determined by inductively coupled plasma (ICP) techniques. The oxidation state of Fe required a separate titration. H_2O^+, H_2O^-, and CO_2 are combined in loss on ignition (LOI). Sr, Ba, Th, Rb, Nb, Y, Hf, Ta, U, Pb, and Cs and 14 rare-earth elements (REEs) were determined by inductively coupled plasma mass spec-

Table 1. Analyses performed on samples for this chapter.

Core, section, interval (cm)	Major elements	REE	XRD		Thin section
			Whole rock	Clays	
149-897C-					
64R-4, 16–19					x
65R-1, 19–23					x
65R-1, 76–80			x	x	x
65R-1, 92–94					
65R-3, 43–47			x	x	x
149-897D-					
7R-3, 5–10	x	x			
10R-4, 144–147			x		x
11R-2, 142–145			x		x
11R-2, 145–150	x	x			
11R-4, 23–25					x
12R-1, 63–65					x
12R-2, 53–60	x	x			
12R-2, 64–68	x	x	x		x
13R-5, 57–61					x
13R-6, 0–4	x	x	x		x
13R-6, 35–41	x	x			
14R-3, 10–14			x	x	x
14R-3, 53–58	x	x			
14R-4, 12–18	x	x			
14R-4, 62–67			x	x	x
15R-1, 16–22					x
15R-1, 32–38	x	x			
16R-3, 132–136					
16R-3, 17–19					x
149-899B-					
15R-1, 16–22			x		
15R-3, 75–77					x
15R-5, 31–37	x				
15R-5, 37–41	x		x	x	
15R-5, 75–78					x
15R-5, 78–84	x				
15R-5, 86–89	x		x		
16R-1, 76–78					x
16R-1, 77–81	x				
16R-1, 81–85	x		x	x	x
16R-1, 111–114	x				
16R-1, 124–128	x		x		x
16R-2, 0–5	x		x		x
16R-2, 69–72					x
16R-3, 73–75					x
16R-4, 102–105					x
17R-1, 82–84	x				x
17R-1, 90–95	x				
17R-3, 73–76					x
18R-1, 74–76					x
18R-3, 70–72					x
19R-2, 111–114					x
20R-1, 121–					x
20R-2, 16–20					x
20R-2, 126–130					x
21R-1, 91–96	x				

trometry (ICP-MS). Ba, V, Cr, Ni, Zn, Cu, Pb, and Sr were also determined by ICP, but the results are generally less accurate than the ICP-MS data. The ICP-MS analyses were performed in the geochemical laboratory at Washington State University; ICP analyses were contracted to commercial laboratories (Chemex and XRAL). Ferrous iron titrations were performed at Iowa State.

OBSERVATIONS

Petrography and Mineralogy of Altered Samples

Preserved Serpentinite Minerals

Only small amounts of minerals native to the serpentinitized peridotite remain in the samples selected for this study. The serpentine mineral lizardite is identified on the basis of peaks at 1.53 Å (060 peak) and 1.50 Å (161 and 204 peaks) and is present in variable amounts. Other minerals identified on the basis of XRD are plagioclase and chlorite. Olivine and clinopyroxene are present in trace amounts, as observed in thin sections. Chromium spinel is readily identified in backscattered images and is minor but ubiquitous. All of these minerals developed fracture porosity, most of which is now filled by calcite. In addition, fractures and other crystal defects serve

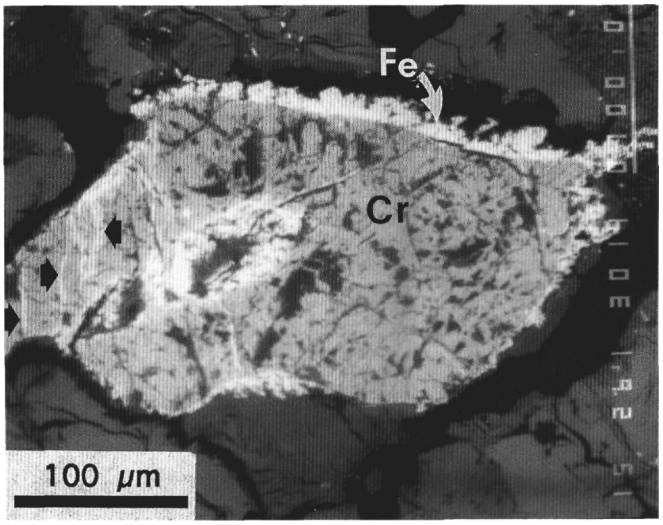

Figure 1. Cr-spinel (Cr) in the highly altered zone that caps the Upper Breccia Unit at Site 899. Fe-oxide cement (Fe) that rims the grain and pervades along small fractures (arrows) and small etch pits (black) attest to a minor degree of spinel alteration through dissolution and replacement. Sample 149-899B-15R-5, 75-78 cm.

to localize clay mineral replacements and vacuolization in serpentine, olivine, and pyroxenes.

Unlike the surviving silicate minerals, chromium spinel shows little or no evidence of fluid interaction beyond serving as a nucleus for the precipitation of some Fe-oxide overgrowths in the highly oxidized zone of Section 149-899-15R-5 (Fig. 1). No volumetrically significant replacement or dissolution of chromium spinel was observed, an observation of key importance for interpretation of the elemental data.

Porosity and Other Evidence of Volume Loss

Basement samples at Sites 897 and 899 are characterized by generally high porosity. Porosity reported for Site 897 basement rocks averages about 20% in Hole 897C (16 measurements) and 16% in Hole 897D (41 measurements) with no apparent depth trend (table 15 in Shipboard Scientific Party, 1994a). At Site 899 basement porosities are also relatively high and manifest a prominent trend with depth (Shipboard Scientific Party, 1994b; Fig. 2). Petrographic observation reveals that much of the porosity in these rocks results from the dissolution of serpentinite minerals (Fig. 3). A few rocks (e.g., Sample 149-899B-16R-4, 102-105 cm) consist essentially of a lattice of calcite veins with intervening secondary porosity.

It is generally unclear whether particular secondary pores result from dissolution of primary peridotite minerals or dissolution of the replacement serpentine. Surviving secondary pores clearly postdate the precipitation of calcite.

Some significant part of both the existing and former porosity is fracture related. The actual contribution of fracture porosity to total porosity is difficult to assess because open natural fractures are not readily preserved during sampling and thin section preparation. As discussed by Morgan and Milliken (this volume), calcite-filled fractures have a complicated crack-seal history, and, thus, open fracture porosity probably never approached the volumetric percentage represented by the present total calcite content.

The decline of carbonate content in the uppermost part of serpentinite breccia at Site 899 and in the immediately overlying zone of clay-rich alteration suggests a late period of dissolution that affected calcite. Carbonate-poor samples from Core 149-899B-16R and possibly from Section 149-899B-15R-5 display evidence of compactional collapse into spaces produced during decarbonation (Fig. 4).

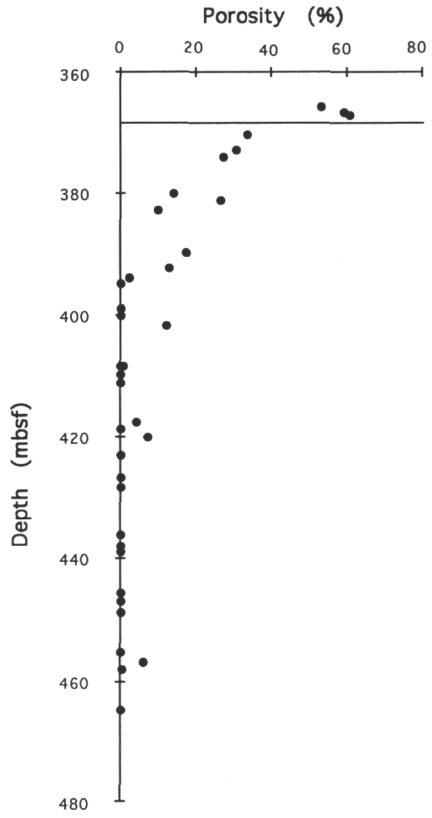

Figure 2. Porosity-depth trend in the Upper Breccia Unit at Site 899. The horizontal line marks the boundary between the heavily oxidized zone in Section 149-899B-15R (three uppermost samples) and the underlying serpentinite breccia. The plotted data extend to the base of the Upper Breccia Unit of lithostratigraphic Subunit IVA at Site 899 (Shipboard Scientific Party, 1994b). In thin section, the enhanced porosity near the top of the Breccia Unit is seen to be related to postcalcitization silicate dissolution, which produces substantial secondary porosity. Data from Shipboard Scientific Party (1994b; table 18).

The latest generation of fractures is filled with detrital fragments, including serpentinite, coarsely crystalline calcite similar to that in veins, and Fe-oxides, ranging in size from clay to granules (Fig. 5). In some late fractures, particles are suspended in a matrix of a pelleted micritic calcite that resembles a possible "internal sediment" similar to those described in Alpine ophiolites (Bernoulli and Weissert, 1985). No fossils have been identified in this material, however.

Authigenic Minerals

Authigenic minerals identified within the altered serpentinites include Fe-oxides of variable oxidation and hydration states, calcite, minor aragonite, minor quartz, minor palygorskite, minor brucite, and Mg-Fe-smectite. Iowaite is present in basement rocks at Site 897 (Shipboard Scientific Party, 1994a; Gibson et al., this volume) but is not present in the samples examined in this study.

Carbonates, low-Mg calcite, with very minor aragonite, precipitated mostly within brittle fractures at both sites (Morgan and Milliken, this volume; Milliken and Morgan, this volume). Replacement calcite is locally abundant (Fig. 6) but, overall, volumetrically minor in comparison to vein fills. Replacement fabrics (calcite localized in serpentinite, olivine, and pyroxene aside from that in transcrystalline brittle fractures) suggest that periods characterized by silicate dissolution and calcite precipitation overlapped.

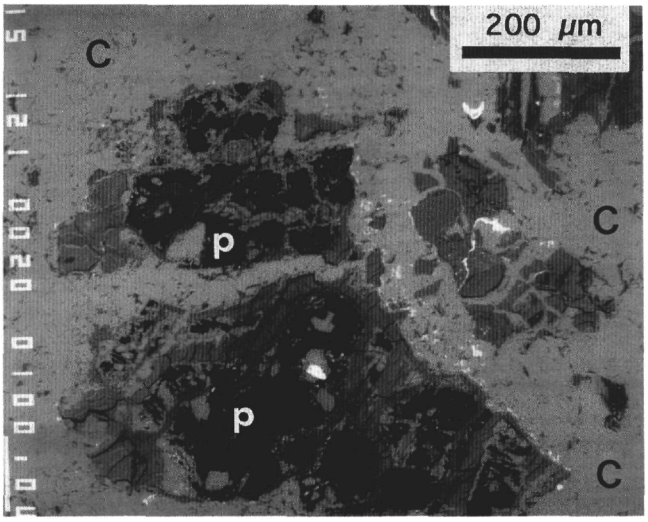

Figure 3. Secondary porosity (p) within partially dissolved serpentinite fragments. The serpentinite is also partially replaced by calcite (C), which cements this highly extended breccia fabric. Blue-dyed impregnation epoxy that fills these pores is proof that this porosity is not an artifact of sample preparation. Though not readily visible in this image, the variable brightness within the serpentinite fragments is related to partial replacement by smectitic clay minerals. Backscattered electron image. Sample 149-897D-15R-1, 16-22 cm.

Calcite volumes in the upper parts of the basement are significant, averaging about 30% (18 samples) in the top 20 m of basement at Site 897 (Hole 897D) and about 25% (27 samples) in the upper 30 m of basement at Site 899 (Shipboard Scientific Party, 1994a, 1994b; data from tables 11 and 8, respectively). Stable isotopic analyses (carbon, oxygen, and strontium) suggest that vein-filling carbonates at both sites precipitated from relatively unmodified seawater at low temperatures (between 10° and 20°C; Milliken and Morgan, this volume).

Reflected-light observation and XRD examination suggest that goethite is volumetrically the most important authigenic Fe mineral. It is present at both sites, but more abundant at Site 897. Variations of color in reflected light and of brightness in backscattered images also suggest the presence of the amorphous limonitic material (yellow in reflected light and darker in backscattered images) and minor hematite (red in reflected light and brighter in backscattered images). Fe-oxides lining some fractures predate the later calcite precipitation. However, given the crack-seal nature of the veins, the timing of calcite vs. Fe-oxide precipitation generally remains unclear (Fig. 7). Zones of oxide inclusions within calcites suggest the overlapping timing of calcite and Fe-oxide precipitation. This observation is discussed further in the section on paragenesis.

The dominant authigenic clay mineral at both sites, but more abundant at Site 899, is an Mg-rich smectite group mineral that contains variable amounts of Fe. The expandable nature of this clay is documented by XRD examination (Fig. 8), whereas the Mg-rich composition is verified by energy-dispersive X-ray observations made during backscattered electron imaging. In backscattered electron images, vein-filling clays typically show prominent zoning that relates to variation in the amounts of Fe and Mg. The presence of a broad XRD peak between 1.51 and 1.52 Å indicates that the expandable clay is probably a mixture of nontronite, saponite, and Fe-rich montmorillonite. Further characterization of the mineral was not possible because abundant fine-grained iron oxides and serpentine prohibited isolation of the smectite.

A second clay mineral characterized by a 10-Å reflection (either illite or glauconite) is suggested in some samples from both sites.

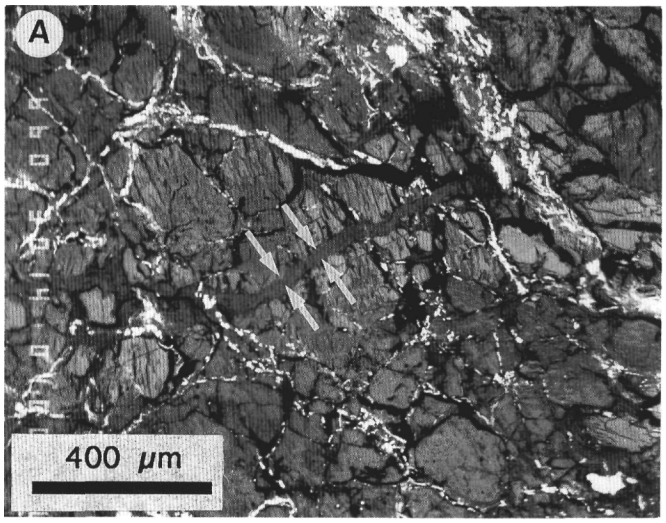

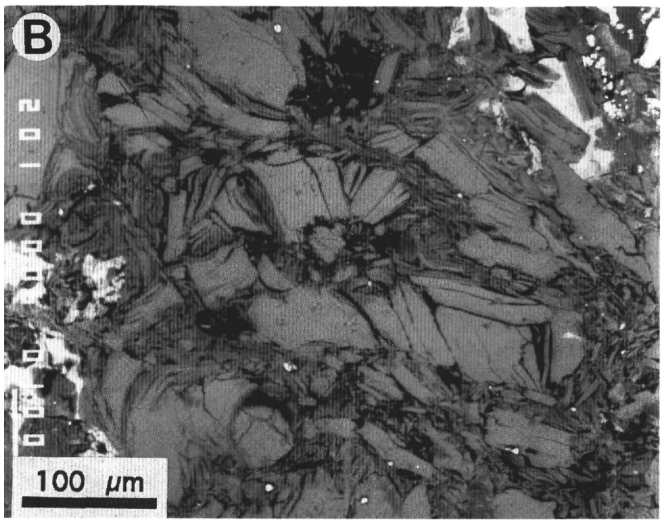

Figure 4. A. Fabric related to carbonate dissolution and intense weathering. Extensive replacement by clays and quartz has left few minerals native to the serpentinite surviving in this sample, although a ghostlike relict of the mesh texture remains. The sample is crosscut by veins filled with clays (e.g., between arrows) and Fe-oxides (very bright). It is possible that calcite, at one time, also filled the veins, but is now removed through dissolution. Backscattered electron image. Sample 149-899B-15R-5, 75-78 cm. B. Fragments of smectite-replaced serpentine separated by zones of finely comminuted serpentine and clay minerals. Zones filled by fine-sized particles (note the very high porosity, black) may at one time have been calcite veins, which are not collapsed. Backscattered electron image. Sample 149-899B-16R-1, 76-78 cm.

Chlorite is present in samples at both sites, but is more abundant at Site 899, especially in the highly altered zone in Section 149-899B-15R-5 immediately above the top of the serpentinite breccia.

Authigenic clay occurs in several habits. Clay replacement of serpentine (Fig. 9), in many cases with partial preservation of the serpentine mesh fabrics, is common throughout the samples examined. In surviving olivine and pyroxene crystals, authigenic clays are localized along fractures and cleavages. A third habit is authigenic clay filling fractures, which are crosscut by later calcite-filled veins or, alternatively, crosscut the calcite veins. Typically, precipitation of fracture-filling clays predated the precipitation of calcite, although the reverse relationship was also observed.

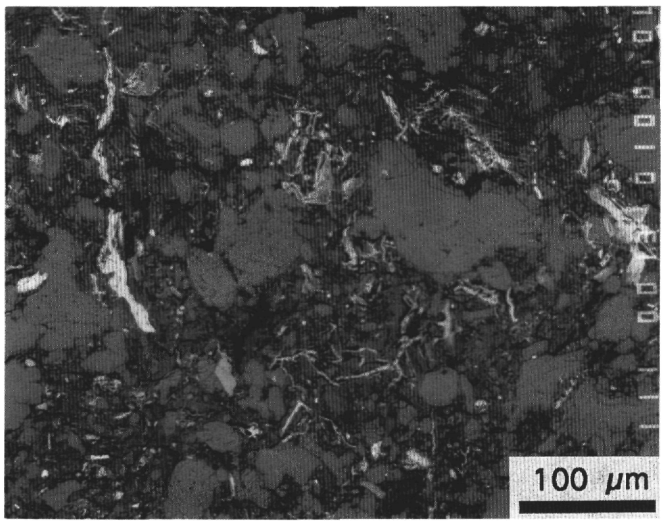

Figure 5. An "internal sediment" of calcite (most of coarser pieces), Fe-oxides, clays, and serpentinite filling a late fracture. Most of the detritus in this vein appears to be material derived from the weathered serpentinte itself. Backscattered electron image. Sample 149-897D-14R-3, 10-14 cm.

Very tentatively identified on the basis of fibrous morphology are small amounts of palygorskite in Section 149-899B-15R-5 (Fig. 10) and in the upper portion of Section 149-899B-16R-1. Palygorskite is difficult to identify by XRD in these samples, because characteristic peaks for palygorskite are masked by those of smectite.

Quartz is present in a distinctive replacement habit, associated with calcite, clay, and small amounts of surviving serpentine (Fig. 11). Quartz appears to have filled discrete regions, possibly representing former secondary pores initially occupied by surviving primary phases surrounded by serpentine. Quartz only partially replaced these minerals, which are typically surrounded by a zone of quartz. Clasts of quartz and calcite having this distinctive replacement fabric are found in the late, detritus-filled veins. Minor authigenic quartz with a fibrous habit is also intergrown with and possibly replaced by calcite in some veins (Morgan and Milliken, this volume).

Trends for Major Elements

Results of whole-rock analyses of major, minor, and trace elements are dominated by the effects of calcitization (Table 2). For example, altered samples at Site 897 average 41.5 wt% CaO, and volatiles make up an average of 34.5 wt%. By comparison, CaO and volatiles in the relatively unaltered serpentinites average 0.39 and 16.0 weight percent, respectively. Similar, though lesser, contrasts exist between altered and unaltered serpentinite breccias at Site 899. To evaluate changes for other elements between altered and unaltered samples, one useful strategy is to calculate values for major elements on a carbonate- and volatile-free basis (Table 3).

One notable contrast between altered and unaltered samples at both sites is the greater concentration of Cr in the altered samples. As discussed in the petrography section, Cr-spinel appears to be relatively stable in the aqueous environment, displaying no evidence of either dissolution or replacement. Cr-spinel is also the predominant reservoir of Cr in the serpentinites (Seifert and Brunotte, this volume). Thus, it is reasonable to use Cr as an "immobile" element against which changes in other elements can be assessed (Table 4). A drawback to this method involves possible primary variation in Cr content between samples selected to represent altered and "unaltered" lithologies.

Mg content in carbonate-free normalizations declines markedly in the unaltered samples, consistent with the observed types and

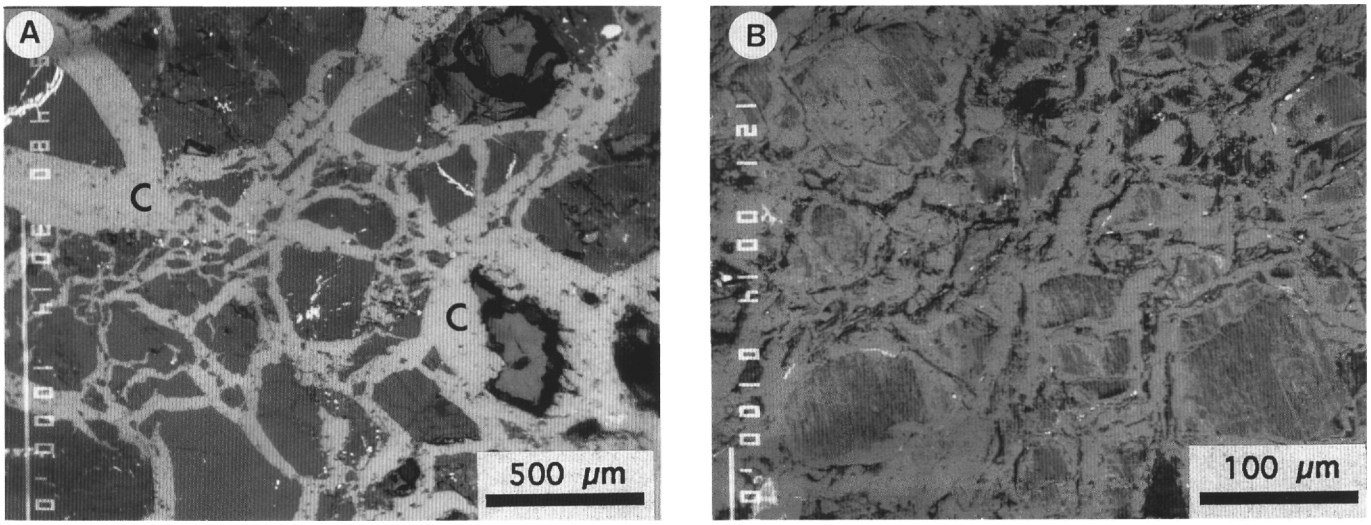

Figure 6. Habits of calcite occurrence. A. Most of the calcite (C) at both sites fills extensional fractures that indicate a significant volume gain. Here, minor post-calcite secondary porosity (black) surrounds some of the serpentinite fragments. See Morgan and Milliken (this volume) for a detailed treatment. Backscattered electron image. Sample 149-899B-16R-3, 73-75 cm. B. Replacement calcite forms by precipitating within a volume formerly occupied by serpentinite minerals. In this example, only ghostlike remnants of serpentine remain in equant and microporous spaces between a myriad of cross-cutting calcite veins. Backscattered electron image. Sample 149-897D-14R-3, 10-14 cm.

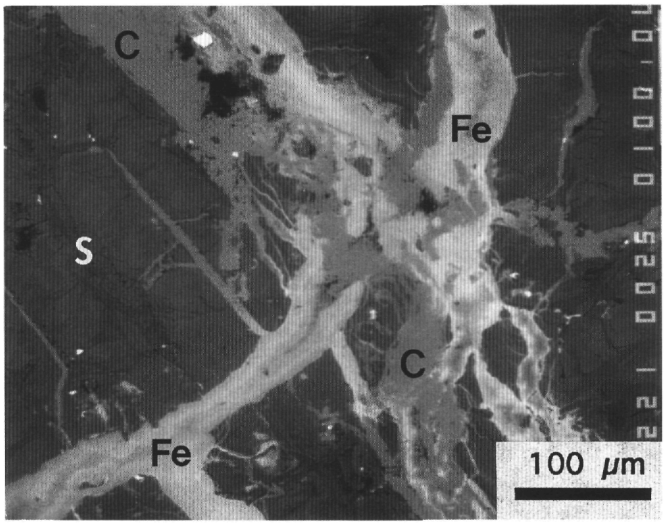

Figure 7. Fracture filled by Fe-oxides (Fe) crosscut with a later fracture filled with calcite (C). The variable brightness of Fe-oxide in this image is related to the variable oxidation/hydration state. Brighter zones are closer to hematite and are red in reflected light, whereas darker zones are compositionally closer to goethite or even limonite and are orange or yellow in reflected light. Backscattered electron image. Sample 149-897D-13R-5, 57-61 cm.

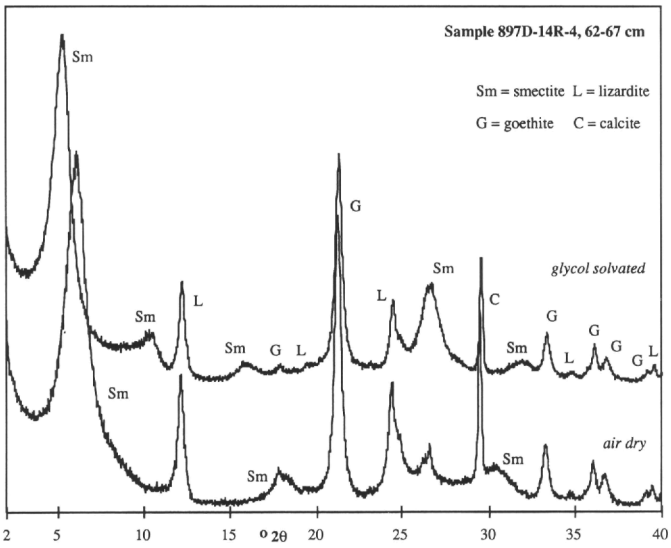

Figure 8. XRD pattern of the <2-μm fraction, oriented and glycolated, of a sample that was not acidified. Sample 149-897D-14R-4, 62-67 cm.

amounts of porosity. Mg in averaged altered serpentinites at Site 897 declines approximately 50% over levels in the unaltered materials. In breccias at Site 899, average Mg content drops by approximately 20% and by about 70% in the highly altered "weathered zone" in Section 149-899B-15R-5.

Assessing Mg decline by comparison with Cr suggests even larger losses overall. At Site 897, Cr-normalized Mg content declines about 74% from levels observed in the unaltered material. Cr-normalized differences between altered and unaltered breccias at Site 899 indicate removal of about 40% of the initial Mg. Cr-normalized Mg loss in the weathered zone is greater than 85% of the amount in the unaltered breccia.

Discrepancies between simple volatile-free and Cr-normalized estimates of Mg loss suggest that some other element, in addition to Ca and CO_2, may be added in significant amounts during alteration. Iron is a candidate for such an element. Oxidized Fe contents are markedly higher in the altered samples. An approximately sixfold increase in oxidized Fe was observed between unaltered and altered serpentinites at Site 897 (volatile-free concentrations). Cr-normalized Fe increase is less, as expected given the decline in Mg, corresponding to an increase of nearly 150%.

Breccias at Site 899 show a threefold increase in oxidized Fe between unaltered and altered materials and an approximate sevenfold increase in the weathered zone. Again, Cr-normalized Fe-increase is less, about twofold in the altered breccia and threefold in the weathered zone. Figure 12 summarizes the covariation of Mg and total Fe

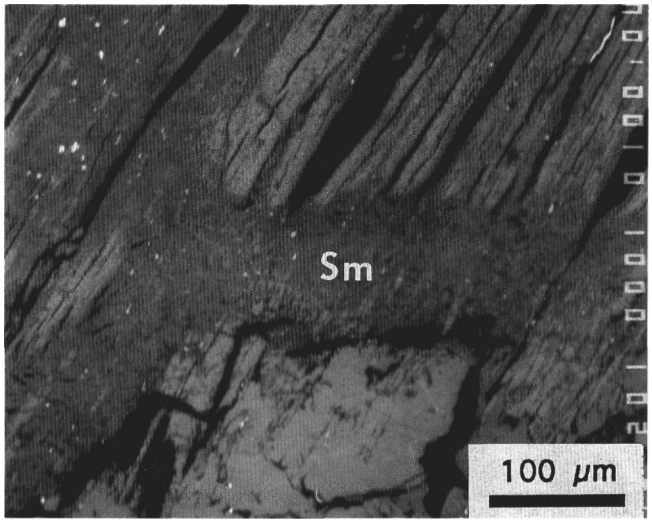

Figure 9. Clay replacement of serpentine. An Mg-Fe smectite (Sm) fills a fracture crosscutting the serpentine (slightly brighter) and also pervades along cleavages. A similar habit of clay replacement was observed in all the highly weathered serpentinites at both Sites 897 and 899. Porosity is black. Backscattered electron image. Sample 149-899B-15R-5, 75-78 cm.

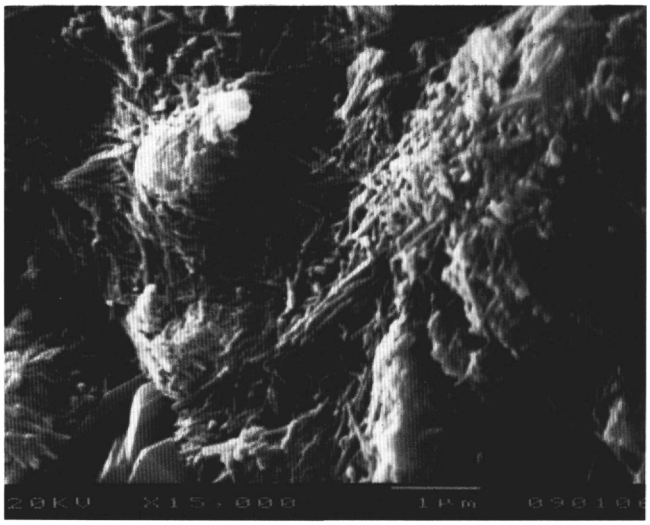

Figure 10. Probable palygorskite, identified on the basis of its fibrous growth habit and Mg-rich composition. Possible palygorskite was also observed in Core 149-899B-16R. Backscattered electron image. Sample 149-899B-15R-5, 86-89 cm.

in the noncarbonate fraction of altered and unaltered rocks at both sites.

Other elements show variations between altered and unaltered materials, but not as significant or as consistent as the changes in Mg and Fe. Assessing the nature of variations for many minor and trace elements is complicated by a lack of information about their dominant reservoirs and the fate of those reservoirs during alteration. For example, Al shows a Cr-normalized decline between unaltered and altered materials at Site 897, but an increase at Site 899. Reservoirs for Al include feldspars (noted by XRD only), pyroxenes (few observed), spinels (present and unaltered), and clay minerals (present in unknown amounts). Al present in clay minerals may represent material mobilized during dissolution of primary minerals, or, alternatively, have been added by circulating fluids. Furthermore, Al could have

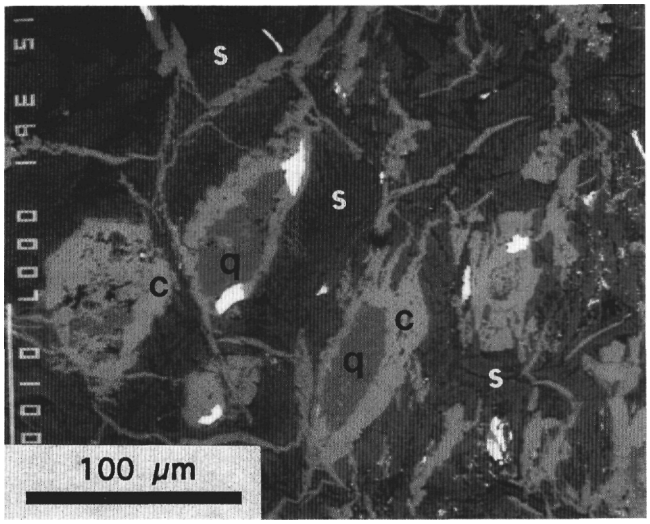

Figure 11. Quartz (q) in a highly replaced serpentine mesh fabric. The quartz probably fills secondary pores left by the dissolution of unserpentinized peridotite minerals. The quartz is surrounded by replacement calcite (c), which also fills brittle fractures. The gray material (s) is an intergrowth of clay and surviving serpentine (not clearly distinguishable in this image). Quartz with this habit and association with calcite was also observed as clasts in some fracture-filling internal sediments. Backscattered electron image. Sample 149-897D-13R-6, 0-4 cm.

been lost from some local regions of the basement rocks at some point in their alteration history, only to be added at another.

Working out the details of such elemental transfers is beyond the scope of the present study. In general, elements that have higher concentrations in the altered rocks are ones that could have been concentrated by virtue of their relative immobility (e.g., Ti) or are plausibly affiliated with volumetrically significant authigenic phases (e.g., Sr, found in aragonite).

Trends for Rare-Earth Elements

REE patterns in the samples examined in this study (Table 5) are contrasted to REE patterns in associated less-weathered (green and indurated) serpentinized peridotite in Figure 13. Heavy rare-earth elements (HREEs) in basement Core 149-897D-19R display a flat pattern (Fig. 13A) with an abundance near 1× chondrite and light rare-earth element (LREE) depletion relative to the chondrite standard. By contrast, weathered serpentinized peridotite, including some blocks recovered above contiguous basement (Cores 149-897D-7R to 15R) have characteristic flat HREE patterns with a large range of abundance, from less than 0.1× chondrite to 4× chondrite, enriched LREE, and large negative Ce anomalies (Fig. 13B, C).

PARAGENESIS

Low-temperature dissolution and precipitation reactions presented in terms of their relative timing in Figure 14 are constructed primarily from evidence observed in thin sections. Brittle deformation and calcitization proceeded through a complex history of repeated fracturing and precipitation (Morgan and Milliken, this volume) that partially overlapped the episodes of Fe-mineral precipitation. Further evidence of the relative timing of Fe oxidation is seen in the positive correlation between the degree of oxidation and the calcium content (among those samples that have not undergone calcite dissolution), which is circumstantial evidence that the same fluids were responsible for calcitization and import of oxidized Fe. Precipitation of all the

authigenic minerals clearly preceded the latest fracturing episodes, because these minerals occur as clasts in the late, detritus-filled fractures. There is some evidence of possible marine carbonate sediment in some of the late fractures, suggesting overlying deposition commenced while some of the later fractures were still open. For a time late in the alteration period, silicates continued to dissolve in the absence of subsequent carbonate precipitation, leaving secondary pores. Carbonate minerals, however, seem to have been mostly immune to this late dissolution. Only in the uppermost part of basement and the overlying weathered zone at Site 899 is there evidence for carbonate dissolution.

DISCUSSION

The alteration process responsible for the textural and compositional modifications described here can reasonably be termed weathering, because of the abundant evidence of oxidation (e.g, Gillis and Robinson, 1988) and considerable volume loss from the silicate portion of the rock. The primary type of chemical reaction affecting the silicate portion of the rock can plausibly be construed as a hydrolysis occurring at very low temperature (see Milliken and Morgan, this volume, for temperature estimates for calcite precipitation), which is perhaps a reaction similar to one suggested by Bonatti et al. (1980):

$$Mg_2SiO_4 + 4H_2O \rightarrow 2Mg^{2+} + 4OH^- + H_4SiO_4,$$

or, alternatively, for serpentine dissolution,

$$Mg_3(Si_2O_5)(OH)_4 + 5H_2O \rightarrow 3Mg^{2+} + 2\ H_4SiO_4 + 6OH^-.$$

Such reactions provide strong silicate buffering that favors the precipitation of carbonate minerals or, in the later stages of alteration, has at least allowed stabilization of carbonates in association with dissolving silicates. The absence of Mg-carbonate phases and the lack of large quantities of authigenic quartz suggest that hydrolysis of serpentinitic materials took place in a highly open chemical system in which materials represented on the right side of the equation were removed in solution and did not strongly influence the fluid composition. Carbonate mineral chemistries further support the idea that subsea weathering of serpentinitic rocks at these sites was characterized by large water/rock ratios (Milliken and Morgan, this volume).

In contrast to Mg, the increase in Fe concentration in the highly weathered samples suggests that Fe mobilized through hydrolysis reactions of Fe-bearing minerals was ultimately sequestered in localized portions of the upper basement through oxidation.

The magnitude of the volume loss suggested by the elemental variations between unaltered and altered materials may provide an explanation of the prominent late fracturing and brecciation observed at both Sites 897 and 899. Calcite resides dominantly in brittle extension fractures (Morgan and Milliken, this volume). The localized volume loss that accompanied secondary dissolution of silicate phases may in part accommodate the volume gain represented by the calcite-filled fractures. Rocks at the top of basement at these sites may be highly fractured because of repeated collapse (either compactional or gravitational) adjacent to localized zones of enhanced volume loss during low-temperature alteration. This proposed genetic association between intense chemical weathering and fracturing is consistent with the high degree of fracturing directly observed in submersible studies at submarine outcrops of ultramafic rocks (e.g., LaGabrielle and Auzende, 1982).

Trends observed for REEs support our interpretation of volumetrically significant alteration by seawater. The REE pattern of the relatively unweathered serpentinites is similar to that expected for depleted mantle (i.e., mantle from which basaltic magma has been extracted). The REE patterns observed in the weathered samples have been previously identified in mafic rocks altered on the seafloor (e.g., Frey et al., 1974; Ludden and Thompson, 1979; Seifert et al., 1985) and are similar to the REE patterns of seawater (Bertram and Elderfield, 1993). The wide range in REE abundance may be caused by the addition or removal of material to the serpentinites, causing relative REE depletion or enrichment, respectively.

CONCLUSIONS

Subsea weathering of serpentinites at Sites 897 and 899 beneath the Iberia Abyssal Plain has caused major textural and compositional modifications in samples that appear altered at the macroscopic scale. The following are our major conclusions concerning the nature and extent of these modifications:

1. The clay-rich zone immediately above the peridotite breccia in Hole 899B represents a weathering profile, enriched in the less mobile components from the underlying serpentinite breccia.
2. Minerals formed during low-temperature alteration of serpentinitic rocks at Sites 897 and 899 include goethite, hematite, quartz, calcite, aragonite, palygorskite(?), and a smectite, possibly a mixture of saponite, nontronite, and Fe-rich montmorillonite.
3. Although many of the alteration minerals are replacements, in the sense that they fill space formerly occupied by minerals "native" to the serpentinite, all the alteration has occurred through a dissolution/precipitation mechanism.
4. A prominent phase of silicate dissolution, postdating carbonate precipitation, produced locally high amounts of secondary porosity.
5. Prominent elemental fluxes including substantial addition of Ca, CO_2, and Fe, considerable loss of Mg, and addition of REEs characteristic of seawater attest to a highly "open" chemical system during low-temperature alteration of the serpentinized peridotite.
6. Much brecciation postdated carbonate precipitation, because vein fragments occur along with particulate Fe-oxides in sediment filling the latest generation of fractures.
7. Carbonate dissolution is a late event that is manifest only in the above-described weathering profile and in the upper part of basement at Site 899.

ACKNOWLEDGMENTS

This study was supported by USSSP 012 to KLM and USSSP 040 to KES. We appreciate the helpful comments of reviewers D.R. Pevear and R.G. Coleman.

REFERENCES

Agrinier, P., Mével, C., and Girardeau, J., 1988. Hydrothermal alteration of the peridotites cored at the ocean/continent boundary of the Iberian Margin: petrologic and stable isotope evidence. *In* Boillot, G., Winterer, E.L., et al., *Proc. ODP, Sci. Results,* 103: College Station, TX (Ocean Drilling Program), 225-234.

Alt, J.C., and Honnorez, J., 1984. Alteration of the upper oceanic crust, DSDP Site 417: mineralogy and chemistry. *Contrib. Mineral. Petrol.,* 87:149-169.

Bernoulli, D., and Weissert, H., 1985. Sedimentary fabrics in Alpine ophicalcites, South Pennine Arosa Zone, Switzerland. *Geology,* 13:755-758.

Bertram, C.J., and Elderfield, H., 1993. The geochemical balance of rare earth elements and neodymium isotopes in the oceans. *Geochim. Cosmochim. Acta,* 57:1957-1986.

Table 2. Whole-rock elemental data, reported in wt%.

Core, section, interval (cm)	SiO_2	TiO_2	Al_2O_3	Cr_2O_3	Fe_2O_3	FeO	MnO	MgO	NiO	CaO	Na_2O
149-897D-											
Unaltered serpentinite											
19R-1, 42–44	33.2	0.03	1.89	0.33	2.56	3.65	0.09	40.5	0.21	0.13	0.10
19R-1, 95–101	31.5	0.08	6.72	0.35	2.42	2.97	0.13	38.6	0.12	0.12	0.03
19R-1, 116–120	30.9	0.09	3.52	1.02	1.46	2.64	0.09	40.5	0.10	0.24	0.13
19R-2, 89–98	33.3	0.05	3.27	0.75	1.89	3.30	0.10	39.9	0.16	0.18	0.17
19R-4, 114–116	33.8	0.13	7.76	0.94	3.19	4.40	0.13	33.3	0.18	0.84	0.10
19R-5, 107–113	37.0	0.09	6.93	0.56	2.51	4.08	0.12	31.5	0.17	3.88	0.06
20R-1, 64–71	35.6	0.02	0.78	0.21	4.46	2.82	0.09	40.5	0.23	0.19	0.09
20R-2, 88–94	35.4	0.02	0.97	0.20	4.66	2.75	0.09	40.5	0.22	0.16	0.09
20R-3, 5–8	34.5	0.15	8.91	0.31	2.64	3.15	0.14	33.9	0.11	1.10	0.07
21R-1, 34–39	33.8	0.02	0.47	0.26	3.77	2.96	0.09	40.4	0.23	0.14	0.21
21R-2, 42–48	33.8	0.00	0.49	0.23	3.93	2.43	0.09	40.7	0.21	0.15	0.27
21R-3, 62–68	33.9	0.02	0.36	0.19	5.20	1.81	0.10	41.4	0.23	0.13	0.18
21R-4, 72–78	33.5	0.01	0.54	0.30	3.83	2.59	0.09	40.9	0.22	0.15	0.22
23R-1, 53–58	32.7	0.02	0.24	0.30	4.66	2.90	0.09	41.1	0.27	0.11	0.04
23R-2, 66–72	32.5	0.02	0.07	0.14	3.92	3.00	0.10	41.1	0.27	0.10	0.07
23R-3, 11–17	34.8	0.02	0.48	0.26	3.85	3.01	0.10	40.2	0.23	0.18	0.08
23R-5, 129–137	35.1	0.01	0.72	0.21	4.05	3.15	0.10	40.1	0.23	0.19	0.15
24R-1, 49–55	33.6	0.03	2.05	0.42	3.99	3.34	0.10	40.2	0.22	0.18	0.10
24R-3, 102–108	33.2	0.01	0.19	0.15	4.40	2.99	0.10	41.6	0.26	0.15	0.05
24R-4, 36–42	32.8	0.01	0.64	0.39	4.35	3.10	0.11	41.5	0.26	0.15	0.07
25R-1, 42–47	34.6	0.01	0.52	0.34	3.26	3.35	0.10	41.0	0.23	0.17	0.10
25R-2, 104–110	34.4	0.01	0.53	0.32	3.61	2.95	0.10	41.2	0.23	0.20	0.03
25R-4, 128–134	34.6	0.01	0.67	0.43	2.81	3.65	0.10	41.3	0.22	0.23	0.03
25R-5, 89–95	34.7	0.00	0.45	0.23	2.76	3.46	0.09	41.5	0.23	0.20	0.02
Average	33.9	0.04	2.05	0.37	3.51	3.10	0.10	39.7	0.21	0.39	0.10
Altered serpentinite											
7R-3, 5–10	6.7	0.05	1.12	0.19	4.63	0.94	0.11	2.1	0.03	46.18	0.15
11R-2, 145–150	8.5	0.00	0.38	0.13	3.29	0.41	0.06	5.4	0.08	44.98	0.09
12R-2, 64–68	6.4	0.04	0.44	0.20	4.30	0.39	0.06	4.6	0.07	46.21	0.01
12R-2, 53–60	5.8	0.01	0.43	0.23	4.19	0.46	0.04	2.7	0.06	47.27	0.09
13R-6, 0–4	3.9	0.04	0.52	0.22	6.56	0.36	0.06	2.5	0.09	47.52	0.02
13R-6, 35–41	20.6	0.01	0.41	0.24	5.69	0.69	0.06	15.1	0.17	29.54	0.13
14R-3, 53–58	18.1	0.02	0.37	0.26	5.51	0.66	0.04	5.1	0.09	38.43	0.07
14R-4, 62–67	8.3	0.25	1.29	0.34	6.47	0.41	0.07	4.6	0.10	43.03	0.08
14R-4, 12–18	27.6	0.03	0.34	0.19	5.43	0.79	0.06	17.0	0.20	22.80	0.05
15R-1, 32–38	2.7	0.00	0.34	0.17	5.16	0.49	0.04	2.1	0.05	49.09	0.06
Average	10.9	0.05	0.56	0.22	5.12	0.56	0.06	6.1	0.09	41.51	0.08
149-899B-											
Unaltered breccia											
19R-1, 26–31	39.0	0.10	2.15	0.32	3.54	2.67	0.06	33.6	0.24	2.97	0.19
19R-4, 92–97	38.7	0.14	2.95	0.29	5.11	1.61	0.08	34.9	0.19	1.84	0.11
20R-1, 127–131	40.5	0.08	1.91	0.35	3.39	3.08	0.06	32.9	0.27	2.02	0.30
20R-4, 7–12	42.9	0.04	1.76	0.38	3.37	4.58	0.09	35.0	0.27	1.47	0.20
21R-4, 1–6	37.4	0.08	1.79	0.22	3.40	2.83	0.07	34.2	0.19	3.70	0.11
21R-5, 22–25	37.0	0.15	2.57	0.25	3.41	3.17	0.07	37.3	0.19	2.30	0.03
21R-5, 82–85	41.6	0.02	1.42	0.40	1.42	5.83	0.11	41.7	0.25	1.29	0.00
25R-2, 105–109	41.2	0.18	4.18	0.48	3.33	0.00	0.09	31.1	0.24	4.00	0.29
Average	39.8	0.10	2.34	0.34	3.37	2.97	0.08	35.1	0.23	2.45	0.15
Altered breccia											
16R-1, 77–81	37.7	0.14	3.96	0.46	11.07	1.92	0.32	25.0	0.23	1.79	0.98
16R-1, 81–85	39.8	0.15	3.75	0.47	9.14	2.55	0.25	24.0	0.23	1.18	0.95
16R-1, 111-114	37.3	0.33	5.87	0.39	8.58	4.69	0.22	25.6	0.21	1.55	0.75
16R-1, 124–128	36.7	0.15	4.24	0.50	11.41	1.49	0.15	24.8	0.22	1.67	0.91
16R-2, 0–5	36.0	0.23	5.26	0.54	17.17	0.85	0.43	22.7	0.26	2.28	0.97
16R-4, 81–84	23.7	0.08	2.34	0.23	5.53	0.55	0.08	18.3	0.15	23.70	0.34
17R-1, 90–95	26.3	0.08	1.81	0.25	5.48	0.43	0.06	21.3	0.15	19.82	0.28
21R-1, 91–96	33.0	0.08	1.97	0.22	5.06	1.12	0.09	30.0	0.18	9.52	0.15
Average	33.8	0.16	3.65	0.38	9.18	1.70	0.20	24.0	0.20	7.69	0.67
Altered zone above breccia											
15R-5, 31-37	33.1	0.39	9.28	0.90	26.05	2.20	0.58	9.0	0.18	0.95	1.65
15R-5, 37–41	36.0	0.37	9.43	0.76	28.37	2.17	0.33	8.3	0.15	1.41	1.76
15R-5, 78-84	31.7	0.44	9.09	0.73	21.76	3.88	0.51	13.8	0.22	1.63	1.19
15R-5, 86–89	32.3	0.51	10.83	0.66	18.38	4.18	0.77	13.6	0.22	4.69	1.05
Average	33.3	0.43	9.66	0.76	23.64	3.11	0.55	11.2	0.19	2.17	1.41

Bonatti, E., Lawrence, J.R., Hamlyn, P.R., and Breger, D., 1980. Aragonite from deep sea ultramafic rocks. *Geochim. Cosmochim. Acta,* 44:1207-1214.

Evans, C.A., and Baltuck, M., 1988. Low-temperature alteration of peridotite, Hole 637A. *In* Boillot, G., Winterer, E.L., et al., *Proc. ODP, Sci. Results,* 103: College Station, TX (Ocean Drilling Program), 235-239.

Frey, F.A., Bryan, W.B., and Thompson, G., 1974. Atlantic Ocean floor: geochemistry and petrology of basalts from Legs 2 and 3 of the Deep Sea Drilling Project. *J. Geophys. Res.,* 79:5507-5527.

Gillis, K.M., and Robinson, P.T., 1988. Distribution of alteration zones in the upper oceanic crust. *Geology,* 16:262-266.

LaGabrielle, Y., and Auzende, J.-M., 1982. Active in situ disaggregation of oceanic crust and mantle on Gorringe Band: analogy with ophiolitic massives. *Nature,* 297:490-493.

Ludden, J.N., and Thompson, G., 1979. An evaluation of the behavior of the rare earth elements during the weathering of sea floor basalt. *Earth Planet. Sci. Lett.,* 43:85-92.

Moore, D.M., and Reynolds, R.C., Jr., 1989. *X-ray Diffraction and the Identification and Analysis of Clay Minerals:* Oxford (Oxford Univ. Press).

Seifert, K.E., Cole, M.R.W., and Brunotte, D.A., 1985. REE mobility due to alteration of Indian Ocean basalt. *Can. J. Earth Sci.,* 22:1884-1887.

Table 2 (continued).

K_2O	P_2O_5	LOI	Total	Fe Total	$Fe^{3+/2+}$	Ba	Cu	Zn	Co	Sr	Zr	Sc	Ta
0.10	0.09	16.8	99.65	5.96	0.70	<5	<10	45	86	<10	<10	8	<20
0.00	0.09	16.2	99.37	5.15	0.81	<5	<10	39	57	<10	<10	24	<20
0.00	0.08	18.8	99.52	3.95	0.55	<5	14	31	46	<10	<10	23	<20
0.20	0.10	16.0	99.38	5.00	0.57	<5	10	35	69	<10	<10	17	<20
0.17	0.06	14.0	98.96	7.27	0.73	5	12	56	89	10	<10	27	24
0.10	0.06	12.0	99.02	6.35	0.62	<5	<10	45	75	<10	<10	26	<20
0.00	0.09	14.4	99.44	6.84	1.58	<5	<10	47	94	<10	<10	4	<20
0.00	0.11	14.4	99.60	6.95	1.69	<5	<10	45	93	<10	<10	4	21
0.09	0.09	14.4	99.50	5.53	0.84	<5	<10	45	62	10	<10	40	<20
0.00	0.10	17.2	99.57	6.35	1.27	<5	22	42	92	<10	<10	6	21
0.08	0.12	17.2	99.72	5.97	1.62	<5	17	37	86	<10	<10	6	<20
0.00	0.10	17.0	100.59	6.50	2.87	<5	<10	40	91	<10	<10	6	<20
0.09	0.10	17.2	99.69	6.04	1.48	<5	<10	42	89	<10	<10	6	27
0.00	0.09	17.0	99.47	7.10	1.61	<5	31	48	105	<10	<10	3	<20
0.00	0.17	18.4	99.87	6.53	1.31	<5	10	38	105	<10	<10	3	50
0.00	0.11	16.2	99.56	6.48	1.28	<5	17	42	89	<10	<10	6	<20
0.00	0.11	15.6	99.74	6.80	1.29	<5	16	42	93	<10	<10	7	28
0.15	0.08	15.2	99.66	6.94	1.19	<5	<10	54	97	<10	<10	8	<20
0.09	0.11	16.3	99.56	6.95	1.47	<5	<10	46	105	<10	<10	4	<20
0.00	0.11	16.0	99.49	7.02	1.40	<5	<10	56	102	<10	<10	4	25
0.06	0.10	15.8	99.65	6.29	0.97	<5	<10	44	93	<10	<10	5	<20
0.00	0.11	16.0	99.73	6.20	1.22	<5	<10	43	91	<10	<10	6	<20
0.13	0.10	15.4	99.60	6.18	0.77	<5	<10	45	85	<10	<10	6	<20
0.00	0.10	15.8	99.54	5.95	0.80	<5	<10	35	87	<10	<10	5	29
0.05	0.10	15.97	99.58	6.26	1.19	<5	17	43	87	10	<10	11	28
0.05	0.14	37.2	99.63	5.11	4.93	17	15	127	13	103	<10	4	<20
0.00	0.05	36.6	99.94	3.38	8.02	<5	16	58	35	134	<10	4	<20
0.00	0.18	37.5	100.38	4.27	11.03	5	10	63	28	121	<10	4	28
0.00	0.05	38.5	99.81	4.24	9.11	5	26	51	38	131	<10	3	<20
0.00	0.08	38.0	99.81	6.27	18.22	<5	32	83	40	109	34	6	<20
0.00	0.09	27.0	99.67	5.81	8.25	<5	<10	73	67	120	<10	5	<20
0.12	0.05	31.0	99.81	5.63	8.35	<5	12	67	31	102	<10	4	<20
0.14	0.18	34.5	99.77	6.24	15.78	<5	<10	75	68	82	<10	5	<20
0.00	0.08	25.0	99.52	5.68	6.87	<5	33	105	53	120	<10	9	<20
0.00	0.10	39.6	99.89	5.14	10.53	<5	13	80	22	103	10	4	<20
0.03	0.10	34.5	99.82	5.18	10.11	<5	20	78	40	113	<10	5	<20
0.16	0.12	16.6	99.50	10.8	3.58	6	57	233	342	59	22	17	<20
0.12	0.10	14.4	99.52	6.14	1.10	<5	11	50	106	27	<10	11	<20
0.12	0.09	9.0	99.33	7.61	0.74	<5	17	55	107	18	<10	12	<20
0.14	0.08	15.4	99.55	5.90	1.20	<5	<10	35	76	19	19	7	<20
0.13	0.12	14.0	100.71	6.25	1.08	18	16	39	79	18	92	9	<20
0.19	0.04	5.3	99.35	7.11	0.24	<5	29	43	98	18	92	9	<20
0.00	0.08	10.4	95.69	7.01	?	20	11	63	103	51	<10	15	20
0.14	0.09	12.08	99.18	6.51	1.13	15	16	47	93	25	49	10	25
0.13	0.13	15.6	99.51	11.9	5.77	8	54	252	284	68	17	16	<20
0.30	0.09	14.5	99.60	5.86	1.33	<5	10	48	94	27	12	10	29
0.30	0.12	13.6	99.69	6.21	3.17	6	<10	45	77	21	29	10	<20
0.24	0.12	13.4	99.24	12.4	1.83	<5	63	232	145	51	31	19	<20
0.42	0.12	17.0	99.69	11.8	7.66	7	65	217	110	56	25	16	<20
0.26	0.15	12.0	99.04	16.3	20.20	15	141	275	303	65	24	23	<20
0.08	0.10	24.8	99.94	5.54	10.05	<5	17	92	71	54	15	8	<20
0.16	0.10	23.8	99.98	5.36	12.74	<5	10	66	51	50	16	7	<20
0.00	0.09	18.2	99.67	5.68	4.52	20	11	36	84	38	13	8	<20
0.22	0.12	17.7	99.57	9.97	8.29	11	52	175	174	55	20	14	<20
0.68	0.16	14.4	99.48	25.7	11.84	196	156	431	260	135	34	30	<20
0.80	0.14	9.59	9.48	27.7	13.07	27	102	380	242	142	47	30	25
0.59	0.19	13.6	99.38	23.5	5.61	48	83	290	252	88	97	32	<20
0.44	0.18	11.4	99.22	20.7	4.40	197	80	277	290	89	56	32	22
0.63	0.17	12.2	99.39	24.40	8.73	117	105	345	261	114	59	31	24

Shipboard Scientific Party, 1994a. Site 897. *In* Sawyer, D.S., Whitmarsh, R.B., Klaus, A., et al., *Proc. ODP, Init. Repts.,* 149: College Station, TX (Ocean Drilling Program), 41-113.

———, 1994b. Site 899. *In* Sawyer, D.S., Whitmarsh, R.B., Klaus, A., et al., *Proc. ODP, Init. Repts.,* 149: College Station, TX (Ocean Drilling Program), 147-209.

Smith, K.L., Milnes, A.R., and Eggleton, R.A., 1987. Weathering of basalt: formation of iddingsite. *Clays Clay Miner.,* 35:418-428.

Date of initial receipt: 1 December 1994
Date of acceptance: 22 May 1995
Ms 149SR-222

Table 3. Whole-rock data from Table 2 (reported in wt%) normalized by removing CaO and LOI.

Core, section, interval (cm)	SiO_2	TiO_2	Al_2O_3	Cr_2O_3	Fe_2O_3	FeO	MnO	MgO	NiO	Na_2O	K_2O	P_2O_5
149-897D-												
Unaltered serpentinite												
19R-1, 42–44	40.1	0.04	2.28	0.40	3.09	4.41	0.11	48.97	0.25	0.12	0.12	0.11
19R-1, 95–101	37.9	0.10	8.09	0.42	2.91	3.58	0.16	46.53	0.14	0.04	0.00	0.11
19R-1, 116–120	38.3	0.11	4.37	1.27	1.81	3.28	0.11	50.31	0.12	0.16	0.00	0.10
19R-2, 89–98	40.0	0.06	3.93	0.90	2.27	3.97	0.12	47.99	0.19	0.20	0.24	0.12
19R-4, 114–116	40.1	0.15	9.22	1.12	3.79	5.23	0.15	39.60	0.21	0.12	0.20	0.07
19R-5, 107–113	44.5	0.11	8.34	0.67	3.02	4.91	0.14	37.88	0.20	0.07	0.12	0.07
20R-1, 64–71	41.9	0.02	0.92	0.25	5.26	3.32	0.11	47.71	0.27	0.11	0.00	0.11
20R-2, 88–94	41.6	0.02	1.14	0.24	5.48	3.23	0.11	47.66	0.26	0.11	0.00	0.13
20R-3, 5–8	41.0	0.18	10.61	0.37	3.14	3.75	0.17	40.32	0.13	0.08	0.11	0.11
21R-1, 34–39	41.1	0.02	0.57	0.32	4.58	3.60	0.11	49.08	0.28	0.26	0.00	0.12
21R-2, 42–48	41.1	0.00	0.59	0.28	4.77	2.95	0.11	49.41	0.25	0.33	0.10	0.15
21R-3, 62–68	40.6	0.02	0.43	0.23	6.23	2.17	0.12	49.60	0.28	0.22	0.00	0.12
21R-4, 72–78	40.6	0.01	0.66	0.36	4.65	3.15	0.11	49.67	0.27	0.27	0.11	0.12
23R-1, 53–58	39.7	0.02	0.29	0.36	5.66	3.52	0.11	49.85	0.33	0.05	0.00	0.11
23R-2, 66–72	39.9	0.02	0.09	0.17	4.82	3.69	0.12	50.55	0.33	0.09	0.00	0.21
23R-3, 11–17	41.8	0.02	0.58	0.31	4.63	3.62	0.12	48.36	0.28	0.10	0.00	0.13
23R-5, 129–137	41.8	0.01	0.86	0.25	4.82	3.75	0.12	47.80	0.27	0.18	0.00	0.13
24R-1, 49–55	39.9	0.04	2.43	0.50	4.73	3.96	0.12	47.65	0.26	0.12	0.18	0.09
24R-3, 102–108	40.0	0.01	0.23	0.18	5.29	3.60	0.12	49.99	0.31	0.06	0.11	0.13
24R-4, 36–42	39.4	0.01	0.77	0.47	5.22	3.72	0.13	49.77	0.31	0.08	0.00	0.13
25R-1, 42–47	41.4	0.01	0.62	0.41	3.90	4.00	0.12	49.00	0.27	0.12	0.07	0.12
25R-2, 104–110	41.2	0.01	0.63	0.38	4.32	3.53	0.12	49.34	0.28	0.04	0.00	0.13
25R-4, 128–134	41.2	0.01	0.80	0.51	3.35	4.35	0.12	49.14	0.26	0.04	0.15	0.12
25R-5, 89–95	41.5	0.00	0.54	0.28	3.30	4.14	0.11	49.71	0.28	0.02	0.00	0.12
Average	40.7	0.04	2.46	0.44	4.21	3.73	0.12	47.75	0.25	0.12	0.06	0.12
Altered serpentinite												
7R-3, 5–10	41.3	0.31	6.89	1.17	28.49	5.78	0.68	13.11	0.18	0.92	0.31	0.86
11R-2, 145–150	46.2	0.00	2.07	0.71	17.92	2.23	0.33	29.30	0.44	0.49	0.00	0.27
12R-2, 64–68	38.5	0.24	2.64	1.20	25.79	2.34	0.36	27.41	0.42	0.06	0.00	1.08
12R-2, 53–60	41.2	0.07	3.06	1.64	29.84	3.28	0.28	19.16	0.43	0.64	0.00	0.36
13R-6, 0–4	27.1	0.28	3.64	1.54	45.91	2.52	0.42	17.28	0.63	0.14	0.00	0.56
13R-6, 35–41	47.7	0.02	0.95	0.56	13.19	1.60	0.14	34.89	0.39	0.30	0.00	0.21
14R-3, 53–58	59.5	0.07	1.22	0.86	18.14	2.17	0.13	16.85	0.30	0.23	0.39	0.16
14R-4, 62–67	37.2	1.12	5.80	1.53	29.09	1.84	0.31	20.86	0.45	0.36	0.63	0.81
14R-4, 12–18	53.3	0.06	0.66	0.37	10.50	1.53	0.12	32.79	0.39	0.10	0.00	0.15
15R-1, 32–38	24.5	0.00	3.04	1.52	46.07	4.37	0.36	18.30	0.45	0.54	0.00	0.89
Average	41.7	0.22	3.00	1.11	26.49	2.77	0.31	23.00	0.41	0.38	0.13	0.54
149-899B-												
Unaltered breccia												
19R-1, 26–31	47.5	0.12	2.62	0.39	4.31	3.25	0.07	40.89	0.29	0.23	0.19	0.11
19R-4, 92–97	45.9	0.17	3.50	0.34	6.07	1.91	0.09	41.38	0.23	0.13	0.14	0.14
20R-1, 127–131	48.8	0.10	2.30	0.42	4.08	3.71	0.07	39.60	0.32	0.36	0.14	0.12
20R-4, 7–12	48.3	0.05	1.98	0.43	3.79	5.15	0.10	39.43	0.30	0.23	0.16	0.10
21R-4, 1–6	46.5	0.10	2.22	0.27	4.23	3.52	0.09	42.47	0.24	0.14	0.16	0.10
21R-5, 22–25	43.8	0.18	3.04	0.30	4.04	3.76	0.08	44.18	0.23	0.04	0.23	0.14
21R-5, 82–85	44.8	0.02	1.53	0.43	1.53	6.29	0.12	44.98	0.27	0.00	0.00	0.04
25R-2, 105–109	48.3	0.21	4.90	0.56	3.90	4.70	0.11	36.47	0.28	0.34	0.16	0.09
Average	46.7	0.12	2.76	0.39	3.99	4.04	0.09	41.17	0.27	0.18	0.15	0.11
Altered breccia												
16R-1, 77–81	45.8	0.17	4.82	0.56	13.48	2.34	0.39	30.39	0.28	1.19	0.37	0.16
16R-1, 81–85	48.7	0.18	4.59	0.58	11.18	3.12	0.31	29.42	0.28	1.16	0.37	0.15
16R-1, 111–114	44.2	0.39	6.96	0.46	10.18	5.56	0.26	30.40	0.25	0.89	0.28	0.14
16R-1, 124–128	45.2	0.19	5.23	0.62	14.08	1.84	0.19	30.55	0.27	1.12	0.52	0.15
16R-2, 0–5	42.4	0.27	6.21	0.64	20.26	1.00	0.51	26.73	0.31	1.14	0.31	0.18
16R-4, 81–84	46.0	0.16	4.55	0.45	10.75	1.07	0.16	35.56	0.29	0.66	0.16	0.19
17R-1, 90–95	46.6	0.14	3.21	0.44	9.72	0.76	0.11	37.79	0.27	0.50	0.28	0.18
21R-1, 91–96	45.9	0.11	2.74	0.31	7.03	1.56	0.13	41.70	0.25	0.21	0.00	0.13
Average	45.6	0.20	4.79	0.51	12.09	2.16	0.25	32.82	0.27	0.86	0.29	0.16
Altered zone above breccia												
15R-5, 31–37	39.4	0.46	11.03	1.07	30.96	2.62	0.69	10.64	0.21	1.96	0.81	0.19
15R-5, 37–41	40.6	0.42	10.65	0.86	32.03	2.45	0.37	9.38	0.17	1.99	0.90	0.16
15R-5, 78–84	37.7	0.52	10.80	0.87	25.86	4.61	0.61	16.41	0.26	1.41	0.70	0.23
15R-5, 86–89	38.9	0.61	13.03	0.79	22.11	5.03	0.93	16.37	0.26	1.26	0.53	0.22
Average	39.1	0.50	11.38	0.90	27.74	3.68	0.65	13.20	0.23	1.66	0.74	0.20

Table 4. Cr-normalized changes, reported in wt% of oxides, between "fresh" and altered materials.*

Rock type:	Serpentine	Altered serpentine	% of initial	Breccia	Altered breccia	% of initial	Breccia	Section 149-899B-15R-5	% of initial
Number:	24	10		8	8		8	4	
SiO_2	33.87	10.85	−46	39.78	33.78	−25	39.78	33.28	−63
TiO_2	0.04	0.05	113	0.10	0.16	38	0.10	0.43	91
Al_2O_3	2.05	0.56	−53	2.34	3.65	37	2.34	9.66	82
Cr_2O_3	0.37	0.22	0	0.34	0.38	0	0.34	0.76	0
Fe_2O_3	3.51	5.12	148	3.37	9.18	139	3.37	23.64	209
FeO	3.10	0.56	−69	3.47	1.70	−57	3.47	3.11	−61
MnO	0.10	0.06	0	0.08	0.20	123	0.08	0.55	207
MgO	39.72	6.11	−74	35.09	23.95	−40	35.09	11.17	−86
NiO	0.21	0.09	−24	0.23	0.20	−22	0.23	0.19	−63
CaO	0.39	41.51	18140	2.45	7.69	176	2.45	2.17	−61
Na_2O	0.10	0.08	24	0.15	0.67	281	0.15	1.41	305
K_2O	0.05	0.03	0	0.13	0.22	55	0.13	0.63	121
P_2O_5	0.10	0.10	71	0.09	0.12	14	0.09	0.17	−18
LOI	15.97	34.49	267	12.08	17.68	29	12.08	12.23	−55
Total	99.58	99.82	70	99.68	99.57	−12	99.68	99.39	−56

Notes: * = averaged data from Table 2; % of initial = percentage change for a given element relative to the amount in the "unaltered" material, assuming no change in Cr.

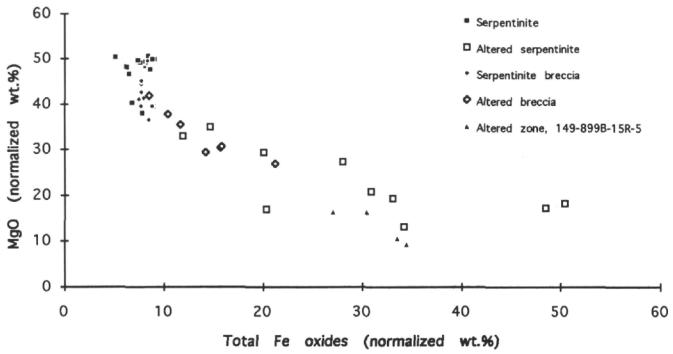

Figure 12. Mg vs. Fe content for both altered and less weathered samples. Values plotted are normalized after removing calcite and volatile components (Table 3).

Table 5. REE data (ppm) for altered and unaltered serpentinites, Site 897.

Core, section, interval (cm)	La	Ce	Pr	Nd	Sm	Eu	Gd	Tb	Dy	Ho	Er	Tm	Yb	Lu
149-897D-														
Altered serpentinites														
7R-3, 5–10	7.9	5.2	1.1	4.2	0.9	0.3	1.1	0.2	1.2	0.3	0.8	0.1	0.6	0.1
11R-2, 145–150	0.5	0.0	0.1	0.1	0.0	0.0	0.0	0.0	0.1	0.0	0.0	0.0	0.0	0.0
12R-2, 53–60	0.7	0.1	0.1	0.1	0.0	0.0	0.0	0.0	0.0	0.0	0.0	0.0	0.0	0.0
12R-2, 64–68	1.7	0.2	0.3	0.8	0.2	0.1	0.2	0.0	0.3	0.1	0.2	0.0	0.2	0.0
13R-6, 0–4	3.4	0.4	0.5	1.7	0.4	0.1	0.5	0.1	0.6	0.1	0.5	0.1	0.4	0.1
13R-6, 35–41	0.3	0.1	0.1	0.1	0.0	0.0	0.0	?	0.0	0.0	0.0	?	0.0	0.0
14R-3, 53–58	0.4	0.1	0.1	0.1	0.0	0.0	0.0	0.0	0.0	0.0	0.0	?	0.0	0.0
14R-4, 12–18	0.3	0.1	0.1	0.1	0.0	0.0	0.0	0.0	0.0	0.0	0.0	?	0.0	0.0
14R-4, 62–67	3.9	1.2	0.6	2.5	0.6	0.2	0.6	0.1	0.7	0.2	0.5	0.1	0.4	0.1
15R-1, 32–38	2.0	0.0	0.2	0.4	0.1	0.0	0.1	0.0	0.2	0.1	0.1	0.0	0.1	0.0
Unaltered serpentinites														
19R-1, 42–44	0.0	0.1	0.0	0.2	0.1	0.1	0.2	0.0	0.3	0.1	0.2	0.0	0.2	0.0
19R-1, 95–101	0.1	0.4	0.1	0.5	0.3	0.1	0.4	0.1	0.7	0.2	0.4	0.1	0.4	0.1
19R-1, 116–120	0.1	0.3	0.1	0.6	0.3	0.1	0.5	0.1	0.8	0.2	0.5	0.1	0.5	0.1

Note: ? = not determined.

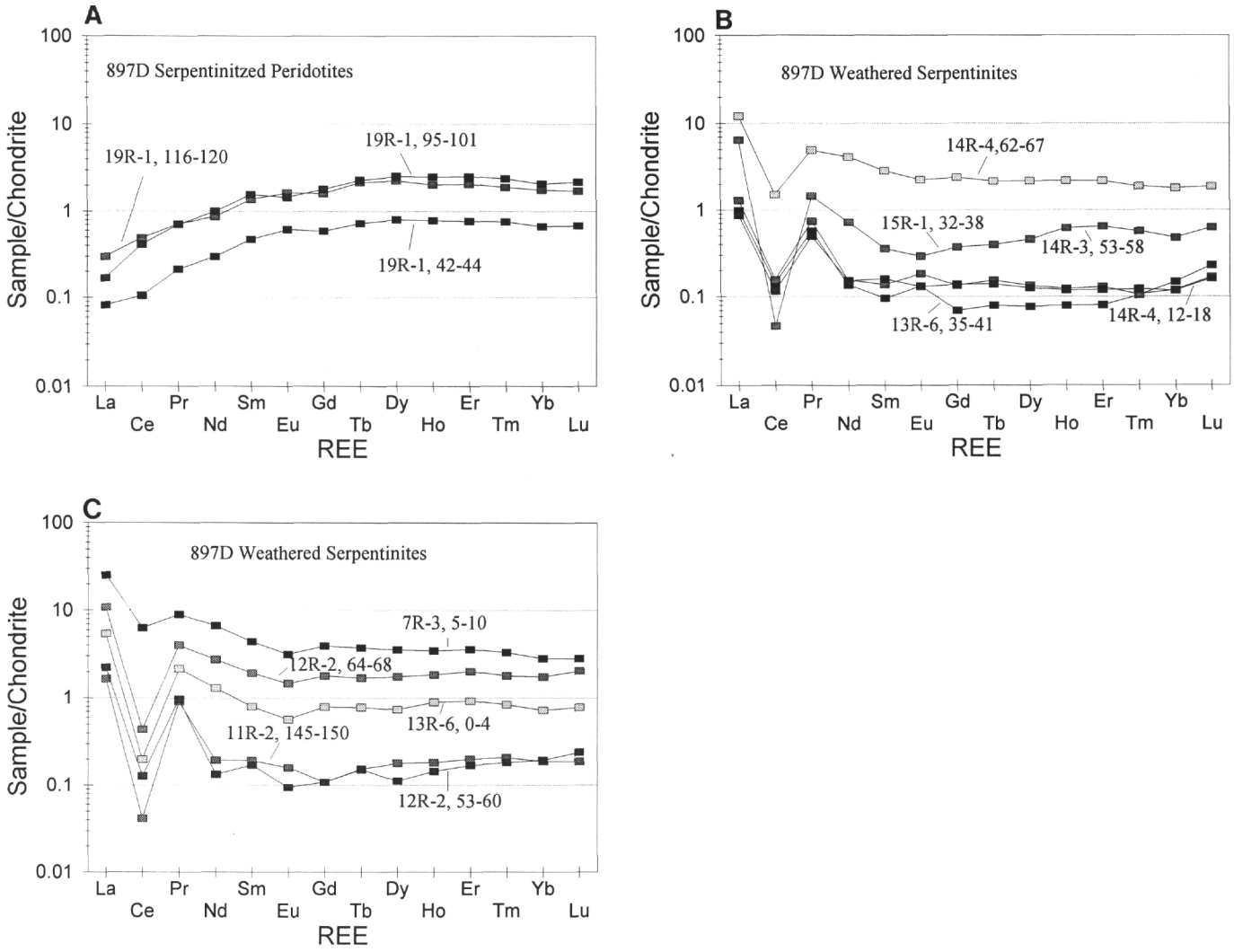

Figure 13. Comparison of REE patterns (relative to the chondrite standard) for less-weathered (**A**) and altered (**B, C**) serpentinized peridotite samples from Site 897.

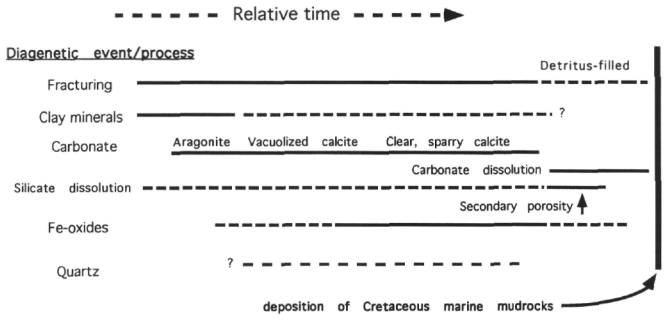

Figure 14. Paragenesis. Relative timing of mineral precipitation and dissolution as observed in thin sections. Information on the timing of different carbonates is summarized from Morgan and Milliken (this volume).